LETTER

Two-photon laser spectroscopy of antiprotonic helium and the antiproton-to-electron mass ratio

Masaki Hori[1,2], Anna Sótér[1], Daniel Barna[2,3], Andreas Dax[2], Ryugo Hayano[2], Susanne Friedreich[4], Bertalan Juhász[4], Thomas Pask[4], Eberhard Widmann[4], Dezső Horváth[3,5], Luca Venturelli[6] & Nicola Zurlo[6]

Physical laws are believed to be invariant under the combined transformations of charge, parity and time reversal (CPT symmetry[1]). This implies that an antimatter particle has exactly the same mass and absolute value of charge as its particle counterpart. Metastable antiprotonic helium ($\bar{p}\mathrm{He}^+$) is a three-body atom[2] consisting of a normal helium nucleus, an electron in its ground state and an antiproton ($\bar{p}$) occupying a Rydberg state with high principal and angular momentum quantum numbers, respectively n and l, such that $n \approx l + 1 \approx 38$. These atoms are amenable to precision laser spectroscopy, the results of which can in principle be used to determine the antiproton-to-electron mass ratio and to constrain the equality between the antiproton and proton charges and masses. Here we report two-photon spectroscopy of antiprotonic helium, in which $\bar{p}\,^3\mathrm{He}^+$ and $\bar{p}\,^4\mathrm{He}^+$ isotopes are irradiated by two counter-propagating laser beams. This excites nonlinear, two-photon transitions of the antiproton of the type $(n, l) \to (n - 2, l - 2)$ at deep-ultraviolet wavelengths ($\lambda = 139.8$, 193.0 and 197.0 nm), which partly cancel the Doppler broadening of the laser resonance caused by the thermal motion of the atoms. The resulting narrow spectral lines allowed us to measure three transition frequencies with fractional precisions of 2.3–5 parts in 10^9. By comparing the results with three-body quantum electrodynamics calculations, we derived an antiproton-to-electron mass ratio of $1{,}836.1526736(23)$, where the parenthetical error represents one standard deviation. This agrees with the proton-to-electron value known to a similar precision.

Antiprotonic atoms (denoted $\bar{p}\mathrm{X}^+$) can be readily synthesized in a given element X by replacing the atomic electrons with a negatively charged antiproton[2]. The substitution takes place spontaneously when antiprotons are brought to rest in the substance concerned. However, these exotic atoms are usually destroyed within picoseconds by electromagnetic cascade mechanisms that result in the annihilation of the antiprotons with the nucleus of X. The $\bar{p}\mathrm{He}^+$ atom alone has microsecond-scale lifetimes even in dense helium targets. The extreme longevity is due to the fact that the antiprotons trapped in the $n \approx l + 1 \approx 38$ Rydberg states have almost no overlap with the nucleus, and furthermore cannot easily de-excite by Auger emission of the electron owing to its large binding energy ($I \approx 25$ eV) and the large multiplicity (Δl) of the necessary transition. The electron protects the antiproton during collisions with other helium atoms, making $\bar{p}\mathrm{He}^+$ amenable to laser spectroscopy.

The energy levels of $\bar{p}\mathrm{He}^+$ have been calculated by three-body quantum electrodynamics (QED) calculations (ref. 3 and V. I. Korobov, personal communication) to precisions of 1×10^{-9}. The calculated values now include nuclear size effects, and relativistic and radiative recoil corrections up to order $m\alpha^6$, where m and α respectively denote the electron mass and the fine structure constant. The fractional measurement precision of single-photon laser spectroscopy experiments[4,5] of $\bar{p}\mathrm{He}^+$, however, has always been limited to 10^{-7}–10^{-8} by the Doppler broadening effect. As in normal atoms, the thermal motion of $\bar{p}\mathrm{He}^+$ at temperature T strongly broadens the measured widths of the laser resonances, by $\sim v\sqrt{8k_B T \log(2)/Mc^2}$, where v denotes the transition frequency, k_B the Boltzmann constant, M the atom's mass and c the speed of light.

One way to reach precisions beyond this Doppler limit is provided by two-photon spectroscopy. For example, the $1s$–$2s$ transition frequency in atomic hydrogen (H) has been measured to a precision of 10^{-14} using two counter-propagating laser beams, each with a frequency of half the $1s$–$2s$ energy interval. This arrangement cancels the Doppler broadening to first order[6]. A similar experiment has been proposed for antihydrogen ($\bar{\mathrm{H}}$) atoms[7,8], a sample of which was recently confined in a magnetic trap[8]. However, it is normally difficult to apply this to $\bar{p}\mathrm{He}^+$ because of the small probabilities involved in the nonlinear transitions of the massive antiproton. Indeed, calculations[9] show that gigawatt-scale laser powers would be needed to excite them against annihilation within the atom's lifetime.

Nevertheless, we have been able to induce two-photon antiproton transitions of the type $(n, l) \to (n - 2, l - 2)$ (Fig. 1a), by using the fact that this small transition probability can be enhanced by factor $>10^5$ if the counter-propagating beams have frequencies, v_1 and v_2, such that the virtual intermediate state of the two-photon transition lies within $\Delta v_d \approx 10$ GHz of a real state[10], $(n - 1, l - 1)$. At resonance between the atom and the laser beams, the antiprotons are directly transferred between the parent and daughter states via the nonlinear transition, leaving the population in $(n - 1, l - 1)$ unaffected. The first-order Doppler width is then reduced by a factor of $|v_1 - v_2|/(v_1 + v_2)$.

In these experiments, transitions were selected for laser excitation between pairs of states with microsecond- and nanosecond-scale lifetimes against Auger emission of the electron. At the two-photon resonance, Auger decay left a $\bar{p}\mathrm{He}^{2+}$ ion behind. No longer protected by the electron in the way described above, the ion was rapidly destroyed in Stark collisions with other helium atoms. Charged pions emerged from the resulting antiproton annihilations, passed through an acrylic sheet and produced Cherenkov radiation, which was detected by photomultipliers. The two-photon resonance condition between the counter-propagating lasers beams and the atom was thus revealed as a sharp spike in the annihilation rate (Fig. 1b).

Even under these conditions of enhanced transition probability, megawatt-scale laser pulses of high spectral purity and low phase noise are needed to excite these two-photon transitions and avoid rapid dephasing of the transition amplitude[10]. For this (Fig. 1c), we developed two sets of Ti:sapphire lasers with pulse lengths of 30–100 ns and among the smallest linewidths reported so far[11] ($\sim$6 MHz). They were based on continuous-wave lasers of wavelength 728–940 nm whose frequencies were measured to a precision of $<1 \times 10^{-10}$ using a femtosecond optical comb[12] locked to a Global-Positioning-System-disciplined quartz oscillator. This continuous-wave seed beam was pulse-amplified to the necessary 1-MW peak power using a Ti:sapphire oscillator and amplifier. Spurious modulations in the pulsed laser frequency, or

[1]Max-Planck-Institut für Quantenoptik, Hans-Kopfermann-Strasse 1, D85748 Garching, Germany. [2]Department of Physics, University of Tokyo, Hongo, Bunkyo-ku, Tokyo 113-0033, Japan. [3]KFKI Research Institute for Particle and Nuclear Physics, H-1525 Budapest, Hungary. [4]Stefan Meyer Institut für Subatomare Physik, Boltzmanngasse 3, Vienna 1090, Austria. [5]Institute of Nuclear Research, H-4001 Debrecen, Hungary. [6]Dipartimento di Chimica e Fisica per l'Ingegneria e per i Materiali, Università di Brescia & Istituto Nazionale di Fisica Nucleare, Gruppo Collegato di Brescia, I-25133 Brescia, Italy.
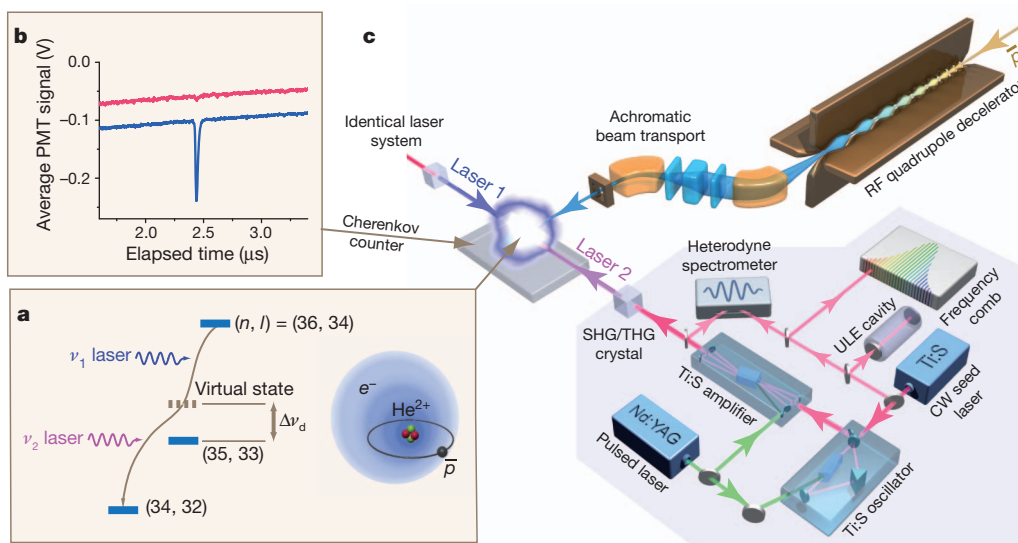
Figure 1 | Energy levels, Cherenkov detector signals and experimental layout for two-photon spectroscopy of $\bar{p}\mathrm{He}^+$. a, Two counter-propagating laser beams induced the two-photon transition $(n, l) = (36, 34) \rightarrow (34, 32)$ in $\bar{p}^4\mathrm{He}^+$ via a virtual intermediate state of the antiproton tuned close to the real state $(35, 33)$. **b**, Cherenkov detectors revealed the annihilation of $\bar{p}^4\mathrm{He}^+$ following the nonlinear two-photon resonance induced at $t = 2.4\,\mu s$ (blue). When one of the lasers was detuned from resonance frequency by $-500\,\mathrm{MHz}$, the two-photon signal abruptly disappeared (red). PMT, photomultiplier tube.

c, The $\bar{p}^4\mathrm{He}^+$ atoms were synthesized by decelerating a beam of antiprotons using a radio-frequency quadrupole, and allowing them to stop in a cryogenic helium target. Two Ti:sapphire pulsed lasers whose optical frequencies were stabilized to a femtosecond frequency comb were used to carry out the spectroscopy. CW, continuous wave; RF, radio frequency; SHG, second-harmonic generation; THG, third-harmonic generation; ULE, ultralow expansion.

'chirp', induced during this amplification are an important source of systematic error[5,13–15] and were measured using a heterodyne spectrometer[11]. The precision of this laser system was verified[11] to be $<1.4 \times 10^{-9}$ by measuring some two-photon transition frequencies in rubidium and caesium at respective wavelengths of 778 and 822 nm.

It was essential to use helium targets of low enough density for the relaxations caused by collisions between $\bar{p}\mathrm{He}^+$ and other helium atoms that could inhibit the two-photon transition to remain small. This implied the use of antiprotons of low enough energy to be stopped in such targets within the volume irradiated by the 2-cm-diameter laser beams. We used the CERN Antiproton Decelerator to produce 200-ns-long, pulsed beams of 5.3-MeV antiprotons (Fig. 1c). Every 100 s, we decelerated about 7×10^6 antiprotons to $\sim$70 keV by allowing them to pass through a 3-m-long, radio-frequency quadrupole decelerator[4]. The beam was then transported by an achromatic, magnetic beamline to the target chamber filled with $^4\mathrm{He}$ or $^3\mathrm{He}$ gas at temperature $T \approx 15\,\mathrm{K}$ and pressure $P = 0.8$–3 mbar. At a time 2–8 μs after the resulting formation of $\bar{p}\mathrm{He}^+$, two horizontally polarized laser beams of energy density $\sim$1 mJ cm^{-2} were simultaneously fired through the target in opposite directions perpendicular to the antiproton beam.

Figure 1b shows the Cherenkov signal (solid blue line) as a function of time elapsed since the arrival of antiproton pulses at the target, averaged over 30 pulses, which corresponds to $\sim$10^7 $\bar{p}\mathrm{He}^+$ atoms. Laser beams of wavelengths $c/v_1 = 417$ and $c/v_2 = 372$ nm were tuned to the two-photon transition $(36, 34) \rightarrow (34, 32)$ such that the virtual intermediate state lay $\Delta v_\mathrm{d} \approx 6\,\mathrm{GHz}$ away from the real state $(35, 33)$. The above-mentioned annihilation spike corresponding to the two-photon transition can be seen at $t = 2.4\,\mu s$. When the 417-nm laser alone was tuned off the two-photon resonance condition slightly (by 0.5 GHz; Fig. 1b, red line), the signal abruptly disappeared as expected. This indicates that the background from any Doppler-broadened, single-photon transitions is very small.

Figure 2b shows the resonance profile measured by detuning the laser of frequency v_2 by $\Delta v_\mathrm{d} = -6\,\mathrm{GHz}$ and scanning the laser of frequency v_1 between -1 and 1 GHz around the two-photon resonance defined by $v_1 + v_2$, which corresponds to a wavelength of $\sim$197.0 nm. The

measured linewidth ($\sim$200 MHz) represents the highest spectral resolution achieved so far for an antiprotonic atom, and is more than an order of magnitude smaller than the Doppler- and power-broadened profile of the corresponding single-photon resonance $(36, 34) \rightarrow (35, 33)$ (Fig. 2a) measured under the same target and laser power conditions. This allows us to determine the atomic transition frequency with a correspondingly higher precision. The remaining width is caused by the hyperfine structure; the 3-ns Auger lifetime of the daughter state, $(34, 32)$; and power broadening effects.

The two-peak structure with a frequency interval of 500 MHz arises from the dominant interaction between the electron spin and the orbital angular momentum of the antiproton. Each peak is a superposition of two hyperfine lines caused by a further interaction between the antiproton and electron spins. The asymmetric structure is reproduced by line shape calculations[9] (see below) and is due to the 25-MHz
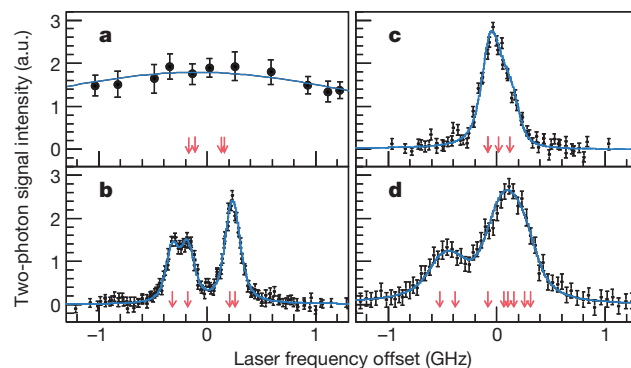

Figure 2 | Profiles of sub-Doppler two-photon resonances. a, Doppler- and power-broadened profile of the single-photon resonance $(36, 34) \rightarrow (35, 33)$ of $\bar{p}^4\mathrm{He}^+$. **b**, Sub-Doppler two-photon profile of $(36, 34) \rightarrow (34, 32)$ involving the same parent state. **c, d**, Profiles of $(33, 32) \rightarrow (31, 30)$ of $\bar{p}^4\mathrm{He}^+$ (**c**) and $(35, 33) \rightarrow (33, 31)$ of $\bar{p}^3\mathrm{He}^+$ (**d**). Black filled circles indicate experimental data points with 1-s.d. error bars, blue lines are best fits of theoretical line profiles (see text) and partly overlapping arrows indicate positions of the hyperfine lines. a.u., arbitrary units.

Table 1 | Spin-averaged transition frequencies of $\bar{p}He^+$

Isotope	Transition $(n, l) \rightarrow (n-2, l-2)$	Transition frequency (MHz)	
		Experiment	Theory
$\bar{p}^4He^+$	$(36, 34) \rightarrow (34, 32)$	1,522,107,062(4)(3)(2)	1,522,107,058.9(2.1)(0.3)
	$(33, 32) \rightarrow (31, 30)$	2,145,054,858(5)(5)(2)	2,145,054,857.9(1.6)(0.3)
$\bar{p}^3He^+$	$(35, 33) \rightarrow (33, 31)$	1,553,643,100(7)(7)(3)	1,553,643,100.7(2.2)(0.2)

Experimental values show respective total, statistical and systematic 1-s.d. errors in parentheses; theoretical values (ref. 3 and V. I. Korobov, personal communication) show respective uncertainties from uncalculated QED terms and numerical errors in parentheses.

spacing between the unresolved hyperfine lines $(S_e, S^{\bar{p}}) = (\uparrow\uparrow) \rightarrow (\uparrow\uparrow)$ and $(\uparrow\downarrow) \rightarrow (\uparrow\downarrow)$ being smaller than the 75-MHz spacing between $(\downarrow\uparrow) \rightarrow (\downarrow\uparrow)$ and $(\downarrow\downarrow) \rightarrow (\downarrow\downarrow)$.

We next detected the $(33, 32) \rightarrow (31, 30)$ resonance at wavelength $\lambda = 139.8$ nm with the lowest n values among the two-photon transitions, using lasers of wavelengths $c/v_1 = 296$ and $c/v_2 = 264$ nm (Fig. 2c). The small transition probability and antiproton population required that higher laser intensities, $P > 2$ mJ cm^{-2}, and small detunings, $\Delta v_d \approx 3$ GHz, from state $(32, 31)$ were needed. For this transition, the four hyperfine lines are much closer together, lying within a 200-MHz range. We also measured the $\bar{p}^3He^+$ resonance $(35, 33) \rightarrow (33, 31)$ at $\lambda = 139.8$ nm (Fig. 2d) using lasers of wavelengths $c/v_1 = 410$ and $c/v_2 = 364$ nm. This profile contains eight partly overlapping hyperfine lines arising from the spin–spin interactions of the ^3He nucleus, the electron and the antiproton.

We determined the spin-independent transition frequencies, v_{exp} (Table 1), by fitting each profile with a theoretical line shape[9] (Fig. 2, blue lines) that was determined by numerically solving the nonlinear rate equations of the two-photon process. This included taking into account all two-photon transitions between the $2l + 1 \approx 70$ substates, the transition rates, power broadening effects, thermal motion of the atoms, the spurious frequency modulation[11] in the laser pulse, the experimentally measured spatial and temporal profiles of the laser beam, and a.c. Stark effects[9]. The positions of the hyperfine lines were fixed to the theoretical values, which have a precision of <0.5 MHz (ref. 16).

For the transition $(36, 34) \rightarrow (34, 32)$ in $\bar{p}^4He^+$ (Table 2), the statistical error, σ_{stat}, due to the finite number of atoms in the laser beam was estimated to be 3 MHz (all quoted errors are s.d.). We measured transitions at various target densities between 1×10^{18} and 3×10^{18} cm^{-3}. Within this density range, no significant collisional shift was observable within the 3-MHz experimental error. This agrees with quantum chemistry calculations (ref. 17 and D. Bakalov et al., personal communication) for which the predictions of 0.1–1-MHz-scale collisional shifts in the associated single-photon lines agreed with experimental results[4,18] to within ~20%. Calculations show that

magnetic Zeeman shifts are also small (<0.5 MHz) for the Rydberg states under our experimental conditions. The frequency chirp of each laser pulse was recorded and corrected to a precision[11] of 0.8 MHz. We estimated the systematic error arising from the calculation of the fitting function[9] to be around 1 MHz.

Laser fields can shift the frequencies of the two-photon transitions[9] by an amount proportional to $(\Omega_1 - \Omega_2)/\Delta v_d$, where Ω_1 and Ω_2 denote the Rabi frequencies of transitions between the parent and virtual intermediate states and, respectively, the daughter and intermediate states. We reduced this a.c. Stark shift to ≤ 5 MHz by carefully adjusting the intensities of the two laser beams such that $\Omega_1 \approx \Omega_2$. Remaining shifts were cancelled to a level of 0.5 MHz by systematically comparing[9] the resonance profiles measured alternately at positive and negative detunings, $\pm\Delta v_d$. The total experimental error, σ_{exp}, was obtained as the quadratic sum of all these errors. The larger error for the 193.0-nm $\bar{p}^3He^+$ transitions is due to the larger number (eight) of hyperfine lines and the smaller signal intensity.

The experimental transition frequencies, v_{exp} (Fig. 3, filled circles with error bars in), agree with theoretical values, v_{th} (squares), to within $(2–5) \times 10^{-9}$. This agreement is a factor of five to ten times better than that obtained in previous single-photon experiments[5]. The calculation uses fundamental constants[19] compiled in CODATA 2002 including the ^3He-to-electron and ^4He-to-electron mass ratios, the Bohr radius and the Rydberg constant. To preserve the independence of this work, we avoided using the more recent CODATA 2006 (http://physics.nist.gov/cuu/Constants/archive2006.html) values, which include results from our previous experiments and three-body QED calculations on $\bar{p}He^+$. The charge radii of the ^3He and ^4He nuclei give corrections to v_{th} of 4–7 MHz, whereas the correction from the antiproton radius is much smaller (refs 3,20; $\ll$ MHz) owing to the large l values of the states. The precision of v_{th} is mainly limited by the uncalculated radiative corrections of order $m\alpha^8$ (Table 2).

When the antiproton-to-electron mass ratio, $M_{\bar{p}}/m_e$, in these calculations was changed by 10^{-9}, v_{th} changed by 2.3–2.8 MHz. By minimizing $\sum_{\bar{p}} [v_{th}(M_{\bar{p}}/m_e) - v_{exp}]^2/\sigma_{stat}^2$, where the sum is over the three $\bar{p}He^+$ frequencies, and considering the above systematic errors, σ_{sys},

Table 2 | Errors for transition $(n, l) = (36, 34) \rightarrow (34, 32)$ of $\bar{p}^4He^+$

Datum	Error (MHz)
Experimental errors	
Statistical error, σ_{stat}	3
Collisional shift error	1
A.c. Stark shift error	0.5
Zeeman shift	<0.5
Frequency chirp error	0.8
Seed laser frequency calibration	<0.1
Hyperfine structure	<0.5
Line profile simulation	1
Total systematic error, σ_{sys}	1.8
Total experimental error, σ_{exp}	3.5
Theoretical uncertainties	
Uncertainties from uncalculated QED terms*	2.1
Numerical uncertainty in calculation*	0.3
Mass uncertainties*	<0.1
Charge radii uncertainties*	<0.1
Total theoretical uncertainty*, σ_{th}	2.1

Experimental errors and theoretical uncertainties are 1 s.d.
* Ref. 3 and V. I. Korobov, personal communication.

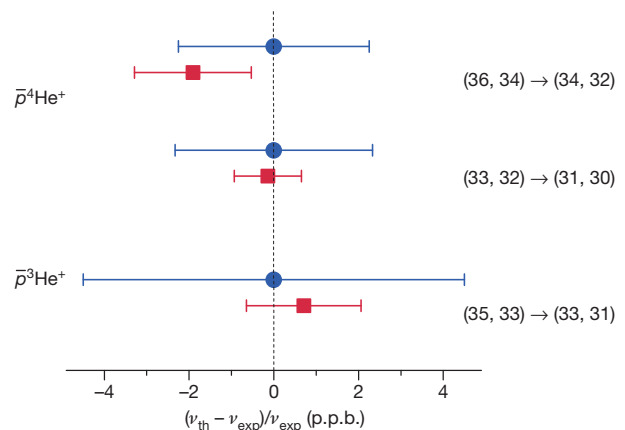**Figure 3 | Two-photon transition frequencies.** The experimental values (v_{exp}; blue circles) for $\bar{p}^4He^+$ and $\bar{p}^3He^+$ agree with theoretical values (v_{th}; red squares) to within fractional precisions of $(2–5) \times 10^{-9}$. Error bars, 1 s.d.; p.p.b., parts per 10^9.
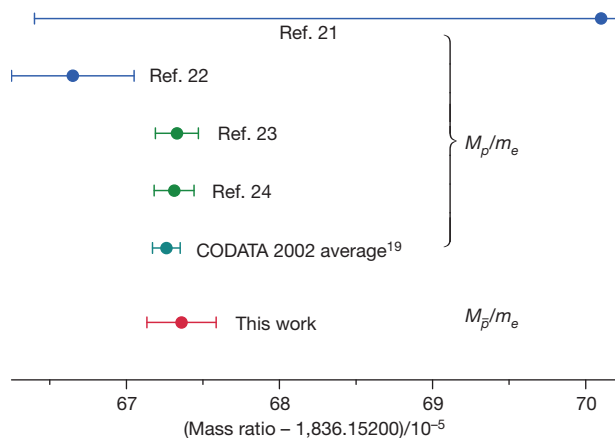
Figure 4 | Antiproton-to-electron and proton-to-electron mass ratios. The antiproton-to-electron mass ratio determined in this work agrees to within a fractional precision of <1.3 p.p.b. with the proton-to-electron values measured in previous experiments[21–24] and the CODATA 2002 recommended value obtained by averaging them[19]. Error bars, 1 s.d.

we obtained the ratio $M_{\bar{p}}/m_e = 1{,}836.1526736(23)$, which yielded the best agreement between theoretical and experimental frequencies. The uncertainty, 2.3×10^{-6}, includes the statistical and systematic experimental contributions, respectively 1.8×10^{-6} and 1.2×10^{-6}, and the theoretical contribution, 1.0×10^{-6}. This is in good agreement with the four previous measurements of the proton-to-electron mass ratio[21–24] (Fig. 4) and has a similar experimental precision. The most precise value for protons is currently obtained by comparing the g factors of hydrogen-like $^{12}C^{5+}$ and $^{16}O^{7+}$ ions measured by the GSI-Mainz collaboration[23,24] with high-field QED calculations. The CODATA recommended value for M_p/m_e is taken as the average over these experiments. This ratio may be determined to higher precision in the future by laser spectroscopy experiments[25] on H_2^+ and HD^+ ions. By assuming[19] CPT invariance, such that $M_{\bar{p}} = M_p = 1.00727646677(10)$ u, we can further derive the value of $m_e = 0.0005485799091(7)$ u for the electron mass from our $\bar{p}He^+$ result.

The equalities between the antiproton and proton charges and masses, formulated respectively as $\delta_Q = (Q_p - Q_{\bar{p}})/Q_p$ and $\delta_M = (M_P - M_{\bar{p}})/M_p$, have been constrained[26,27] to within 2×10^{-5}. This was achieved by combining X-ray spectroscopic data on antiprotonic atoms ($\propto Q_{\bar{p}}^2 M_{\bar{p}}$) with the cyclotron frequency ($\propto Q_{\bar{p}}/M_{\bar{p}}$) of antiprotons confined in Penning traps and measured to a higher precision. We can improve this limit by more than four orders of magnitude by studying the linear dependence[2] of δ_M and δ_Q on v_{th}, that is, $\delta_M\kappa_M + \delta_Q\kappa_Q \leq |v_{exp} - v_{th}|/v_{exp}$. For the three transitions, the constants κ_M and κ_Q were estimated[2] to be 2.3–2.8 and 2.7–3.4, respectively. The right-hand side of the inequality was evaluated to be $<(8 \pm 15) \times 10^{-10}$ by averaging over the three transitions. Furthermore, the constraint that $(Q_{\bar{p}}/M_{\bar{p}})/(Q_p/M_p) + 1 = 1.6(9) \times 10^{-10}$, from the TRAP experiment[28,29], implies that $\delta_Q \approx \delta_M$. From this, we conclude that any deviations between the charges and masses are $<7 \times 10^{-10}$ at the 90% confidence level.

METHODS SUMMARY

The two continuous-wave seed lasers were stabilized relative to 470-mm-long, monolithic cavities made of ultralow-expansion glass by using the Pound–Drever–Hall technique. The cavities were suspended horizontally by springs and isolated in a vacuum chamber whose temperature was stabilized to $\pm 0.05\,^{\circ}C$. Drifts in the laser frequencies were typically <0.1 MHz h^{-1}. The frequency chirp[11,13–15] during pulsed laser amplification was corrected using electro-optic modulators placed inside the pulsed laser resonators, such that its amplitude was reduced to a few megahertz. This remaining chirp was recorded for each laser pulse and its effect corrected for at the data analysis stage. The output beams were

frequency-doubled (second-harmonic generation) or frequency-tripled (third-harmonic generation) to wavelengths of $\lambda = 264$–417 nm in β-barium borate and lithium triborate crystals. Simulations[5,13,14] show that additional chirp caused by this frequency conversion is negligible (<0.1 MHz).

The Cherenkov signals corresponding to $\bar{p}He^+$ were recorded using a digital oscilloscope, and the area under the peak in each of these time spectra (Fig. 1b) was plotted as a function of laser frequency to obtain the resonance profiles in Fig. 2. Each data point represents an average of 8–10 antiproton beam arrivals at the target. This measurement was repeated for 10,000 arrivals at various laser intensities, target densities, frequency offsets (v_d) and alignments of the antiproton beam. The fact that the pulsed laser can maintain absolute precision for the duration of the measurements was verified by using part of the light to measure the $6s$–$8s$ two-photon transition frequency of caesium 20 times over a two-week period. The result, with a conservative error of 1.4×10^{-9}, was in good agreement with previous experiments[30]. The acquired resonance profile was fitted with the theoretical two-photon resonance line shape as described in the main text. This a-priori calculation well reproduced the experimental data (Fig. 2). The validity of this method was also partly verified by using it to analyse the above-mentioned caesium two-photon signal[11].

1. Bluhm, R., Kostelecký, V. A. & Russell, N. CPT and Lorentz tests in hydrogen and antihydrogen. *Phys. Rev. Lett.* **82,** 2254–2257 (1999).
2. Hayano, R. S., Hori, M., Horváth, D. & Widmann, E. Testing CPT invariance with antiprotonic helium. *Rep. Prog. Phys.* **70,** 1995–2065 (2007).
3. Korobov, V. I. Calculations of transitions between metastable states of antiprotonic helium including relativistic and radiative corrections of order $R_\infty \alpha^4$. *Phys. Rev. A* **77,** 042506 (2008).
4. Hori, M. et al. Direct measurement of transition frequencies in isolated $\bar{p}He^+$ atoms, and new CPT-violation limits on the antiproton charge and mass. *Phys. Rev. Lett.* **91,** 123401 (2003).
5. Hori, M. et al. Determination of the antiproton-to-electron mass ratio by precision laser spectroscopy of $\bar{p}He^+$. *Phys. Rev. Lett.* **96,** 243401 (2006).
6. Parthey, C. G. et al. Precision measurement of the hydrogen-deuterium 1s-2s isotope shift. *Phys. Rev. Lett.* **104,** 233001 (2010).
7. Gabrielse, G. et al. Antihydrogen production within a Penning-Ioffe trap. *Phys. Rev. Lett.* **100,** 113001 (2008).
8. Andresen, G. B. et al. Trapped antihydrogen. *Nature* **468,** 673–676 (2010).
9. Hori, M. & Korobov, V. I. Calculation of transition probabilities and ac Stark shifts in two-photon laser transitions of antiprotonic helium. *Phys. Rev. A* **81,** 062508 (2010).
10. Bjorkholm, J. E. & Liao, P. F. Resonant enhancement of two-photon absorption in sodium vapor. *Phys. Rev. Lett.* **33,** 128–131 (1974).
11. Hori, M. & Dax, A. Chirp-corrected, nanosecond Ti:sapphire laser with 6 MHz linewidth for spectroscopy of antiprotonic helium. *Opt. Lett.* **34,** 1273–1275 (2009).
12. Udem, Th., Holzwarth, R. & Hänsch, T. W. Optical frequency metrology. *Nature* **416,** 233–237 (2002).
13. Meyer, V. et al. Measurement of the 1s-2s energy interval in muonium. *Phys. Rev. Lett.* **84,** 1136–1139 (2000).
14. Eikema, K. S. E., Ubachs, W., Vassen, W. & Hogervorst, W. Lamb shift measurement in the 1^1S ground state of helium. *Phys. Rev. A* **55,** 1866–1884 (1997).
15. Bakule, P. et al. A chirp-compensated, injection-seeded alexandrite laser. *Appl. Phys. B* **71,** 11–17 (2000).
16. Korobov, V. I. Hyperfine structure of metastable states in $^3He^+\bar{p}$. *Phys. Rev. A* **73,** 022509 (2006).
17. Bakalov, D., Jeziorski, B., Korona, T., Szalewicz, K., & Tchoukova, E. Density shift and broadening of transition lines in antiprotonic helium. *Phys. Rev. Lett.* **84,** 235–238 (2000).
18. Hori, M. et al. Sub-ppm laser spectroscopy of antiprotonic helium and a CPT-violation limit on the antiprotonic charge and mass. *Phys. Rev. Lett.* **87,** 093401 (2001).
19. Mohr, P. J. & Taylor, B. N. CODATA recommended values of the fundamental constants: 2002. *Rev. Mod. Phys.* **77,** 1–107 (2005).
20. Pohl, R. et al. The size of the proton. *Nature* **466,** 213–216 (2010).
21. Van Dyck, R. S. Jr. Moore, F. L., Farnham, D. L. & Schwinberg, P. B. Improved measurement of proton-electron mass ratio. *Bull. Am. Phys. Soc.* **31,** 244–244 (1986).
22. Farnham, D. L., Van Dyck, R. S. Jr & Schwinberg, P. B. Determination of the electron's atomic mass and the proton/electron mass ratio via Penning trap mass spectroscopy. *Phys. Rev. Lett.* **75,** 3598–3601 (1995).
23. Beier, T. et al. New determination of the electron's mass. *Phys. Rev. Lett.* **88,** 011603 (2002).
24. Verdú, J. et al. Electronic g factor of hydrogenlike oxygen $^{16}O^{7+}$. *Phys. Rev. Lett.* **92,** 093002 (2004).
25. Koelemeij, J. C. J., Roth, B., Wicht, A., Ernsting, I., & Schiller, S. Variational spectroscopy of HD$^+$ with 2-ppb accuracy. *Phys. Rev. Lett.* **98,** 173002 (2007).
26. Hughes, R. J. & Deutch, B. I. Electric charges of positrons and antiprotons. *Phys. Rev. Lett.* **69,** 578–581 (1992).
27. Nakamura, K. et al. Review of particle physics. *J. Phys. G* **37,** 075021 (2010).
28. Gabrielse, G. et al. Precision mass spectroscopy of the antiproton and proton using simultaneously trapped particles. *Phys. Rev. Lett.* **82,** 3198–3201 (1999).

29. Thompson, J. K., Rainville, S. & Pritchard, D. E. Cyclotron frequency shifts arising from polarization forces. *Nature* **430,** 58–61 (2004).
30. Fendel, P., Bergeson, S. D., Udem, Th & Hänsch, T. W. Two-photon frequency comb spectroscopy of the 6s-8s transition in cesium. *Opt. Lett.* **32,** 701–703 (2007).

Author Contributions M.H. designed the two-photon experiment. M.H. and A.D. developed the laser systems and carried out the caesium and rubidium measurements. M.H. and D.B. constructed the cryogenic target. M.H. developed the antiproton beam profile monitors, Cherenkov counters, cryogenic optics and data acquisition system. D.B. and M.H. wrote the analysis software. All authors contributed to the beam-time data taking and analysis. M.H. wrote the manuscript and all authors discussed the results and contributed to the editing.

Author Information Reprints and permissions information is available at www.nature.com/reprints. The authors declare no competing financial interests. Readers are welcome to comment on the online version of this article at www.nature.com/nature. Correspondence and requests for materials should be addressed to M.H. (masaki.hori@mpq.mpg.de).